Construction and Building Materials 438 (2024) 137036

Contents lists available at ScienceDirect

Construction and Building Materials

journal homepage: www.elsevier.com/locate/conbuildmat

Self-healing effect of hydrogels in cement slag and fly ash pastes

Babak Vafaei, Ali Ghahremaninezhad *

Department of Civil and Architectural Engineering, University of Miami, Coral Gables, FL 33146, United States

ARTICLE INFO

Keywords:
Hydrogels
Self-healing
Slag
Fly ash
Cement

ABSTRACT

This paper aims to study the effect of hydrogels on the self-healing processes in cementitious systems with a large dosage of supplementary cementitious materials including slag and fly ash. The material characterization was conducted using thermogravimetric analysis (TGA), Fourier transform infrared spectroscopy (FTIR), and scanning electron microscopy (SEM/EDS). The healing products in the cement slag system consisted primarily of calcium carbonate and hydration products including calcium silicate hydrate (C-S-H) and ettringite. In the cement fly ash system, calcium carbonate and C-S-H/C-A-S-H comprise the main phases in the healing products. It was noticed that the ratio of calcium carbonate to the hydration products was larger in the cement fly ash systems compared to the cement slag systems. The addition of hydrogels resulted in a higher content of calcium carbonate in the healing products of both systems. Hydrogels enhanced the mechanical regain and crack filling in both cement slag and cement fly ash systems compared to the control system without hydrogels.

1. Introduction

The production of one ton of Portland cement (PC) demands 4–5 Gigajoules of energy [1–3] and contributes to 5 % of the global industrial energy consumption [4,5]. Moreover, the production of PC accounts for approximately 9 % of the total human-caused greenhouse gas emissions [5–7]. Consequently, the replacement of PC with industrial wastes with lower embodied energy is demanded in the construction industry to alleviate the environmental repercussions of PC. Ground granulated blast-furnace slag and fly ash, as industrial by-products of the steel and coal industries, respectively, offer potential replacements for PC in concrete structures. Despite the environmental benefits of slag and fly ash, like PC concrete, slag and fly ash cement concrete are brittle composite materials, resulting in cracking when subjected to tensile stresses and shrinkage. Cracking in concrete facilitates the penetration of corrosive substances, including chloride, carbonate, and sulfate. The presence of such corrosive substances results in the corrosion of steel rebars and the deterioration of concrete materials, ultimately diminishing the durability of concrete structures [8]. In the event of advancing damage, the affected members must undergo repair, or in the worst-case scenario, replacement, which requires substantial costs and service interruptions. For instance, approximately 27 % of all highway bridges in the USA require repair or replacement, with estimated corrosion-related deterioration costs exceeding 150 billion dollars [9]. According to U.S. Portland Cement Association [10], in 2015, concrete production in the U.S. reached 92 million tons which translates into $10.6 billion of state revenue. Hence, the development and application of self-healing products represents a viable approach to address the cracking issues and alleviate the environmental and economic impacts associated with concrete structures.

Although slag and fly ash cement concrete are characterized as brittle composite materials, slag and fly ash exhibit a slower reaction rate in concrete compared to cement clinkers [11]. Consequently, a significant portion of slag and fly ash remains unreacted in the mixture for a long time period of time [11]. Continued hydration of the unhydrated slag or fly ash can potentially contribute to self-healing in these mixtures [12–16]. It is well known that slag is activated in a pH range below 12, whereas fly ash required a pH exceeding 13 [17]. To determine the self-healing potential of slag and fly ash, saturated lime solution can be utilized to increase continued hydration of slag and fly ash. Superabsorbent polymer hydrogels can absorb a large amount of solution and retain it without undergoing disintegration [18–25]. The absorbed liquid by hydrogels can be further released into the crack and surrounding cementitious materials and employed for further reaction of the unreacted cementitious particles. Thus, enhancing the action of self-healing within the crack. Hydrogels employed in cementitious materials typically consist of either a cross-linked polymer of acrylate salt or a copolymer of acrylate salt–acrylamide [26]. The beneficial effects of hydrogels on mitigating autogenous shrinkage and enhancing the microstructure and hydration of PC mixtures [20,21,27] and

* Corresponding author.
E-mail address: a.ghahremani@miami.edu (A. Ghahremaninezhad).

https://doi.org/10.1016/j.conbuildmat.2024.137036
Received 9 February 2024; Received in revised form 3 June 2024; Accepted 9 June 2024
Available online 17 June 2024

Table 1
Chemical compositions of the hydrogels used in the experiments.

Hydrogel Designation	AA (g)	AM (g)	APS (g)	MBA (g)	NaOH (g)	Deionized Water (g)
HL-A	10	10	0.128	0.05	1.35	100
HL-B	2	18	0.128	0.05	0.27	100

alkali-activated mixtures [28–33] have been previously investigated. The efficiency of hydrogels to improve resistance against the freeze-thaw [34,35] was previously reported. Studies have also shown that hydrogels can successfully seal the cracks when water flows through the cracks [36–38]. Lee et al. [38] observed that adding 5 % hydrogel reduced cumulative flow from cracks by 80 %. Lee et al. [39] investigated the self - sealing processes of the hydrogels.

Autogenous healing, manifested through the continued reaction of cement, the pozzolanic reactivity of supplementary cementitious materials, and the crystallization of calcium carbonate, has the capability to heal cracks [8,40–42]. The impact of the hydrogels as a self-healing agent in PC binders have previously investigated [8,19,37–39,43–47]. The improvement in self-healing in cement-based binders, incorporating various dosages of hydrogels was investigated in the past [43]. They reported that the optimal results will be achieved in terms of self-healing by introducing 1 % per cement mass of hydrogel. In another study [44], the authors used 3D X-ray microcomputed tomography to investigate the formation of the healing products in the cracks in samples containing hydrogels. The spatial distribution of healing materials in cracks in the mixtures containing bio-based hydrogels was analyzed using X-ray computed microtomography [46]. Lee at al. [45] developed a model for calculating the volumetric percentage of crack filling by hydrogels in cement-based mixtures. The model incorporates variables like crack size, hydrogel dosage and absorption.

Despite several investigations examined the self-healing effects of hydrogels in Portland cement-based mixtures [8,19,37–39,43–46], such hydrogel effects in the systems containing a large amount of supplementary cementitious materials (SCMs) are not well-understood. The reaction conditions within cracks differs from those in the bulk paste. Firstly, when the solution enters the cracks from the exterior, a more substantial amount of solution is available for further reactions with unreacted slag and fly ash present on crack surfaces compared to the bulk paste [8,48–50]. Secondly, in comparison to the bulk paste, there is a significantly larger space within the crack for the precipitation of the reaction products, influencing the minerology and microstructure of the reaction products, as previously observed by [8,48,50]. Thus, the properties of subsequent reactions involving unreacted slag and fly ash can be impacted by these unique conditions within cracks and by adding hydrogels to the slag and fly ash cement pastes. However, investigations focused on the chemical characteristics of healing products and mechanical recovery in the cementitious systems containing hydrogels and with a large amount of slag and fly ash are scarce. Thus, the main aim and novelty of this study is to gain insight into how hydrogels affect the self-healing processes in cementitious systems with a large amount of slag and fly ash.

In this paper, analytical techniques such as Fourier transform infrared spectroscopy (FTIR), thermogravimetric analysis (TGA), and scanning electron microscopy (SEM) equipped with an energy dispersive spectroscopy (EDS) were used for material characterization. Mechanical recovery was evaluated using a three-point bend setup and the filling of the cracks was tracked with optical microscopy.

2. Experiment

2.1. Materials

2.1.1. Hydrogels

Two hydrogels with different chemical compositions were prepared via free radical polymerization [51–59]. The primary monomers used in the synthesis of these hydrogels, HL-A and HL-B, are acrylamide (AM) and acrylic acid (AA), as shown in Table 1. The chemicals utilized in the synthesis of the hydrogels were procured from Sigma-Aldrich. In the first step to synthesizing HL-A and HL-B, 10 g and 2 g of AA were added into 100 g of deionized water, respectively. Then, the solutions were partially neutralized with sodium hydroxide (NaOH), followed by adding AM, the crosslinking agent, N,N'-methylenebisacrylamide (MBA), and the initiator, ammonium persulfate (APS), to the solution. After degassing with argon, the solution was allowed to gel in an oven at 50 °C for 3 hours. Then, the samples were crushed into small pieces, rinsed in distilled water overnight and dried at 60 °C for seven days. Then, the hydrogels were grinded and sieved so that only hydrogel particles in the range of 75–300 μm were used in the slag and fly ash pastes as described next.

Table 2
Chemical composition of Portland cement, slag, and class F fly ash.

Composition	Portland Cement (%)	Slag (%)	Fly Ash (%)
SiO_2	20.8	32.1	54.0
Al_2O_3	5.0	12.9	28.0
Fe_2O_3	3.7	0.8	7.0
CaO	64.2	42.4	1.4
MgO	0.9	6.5	1.0
Na_2O	0.2	0.1	0.3
K_2O	0.4	0.3	2.4
SO_3	2.8	3.0	0.1
TiO_2	0.2	0.6	-
B_2O_3	-	-	-

2.1.2. Mix designs

A type I/II Portland cement (PC), ground granulated blast-furnace slag, and fly ash class F manufactured by CEMEX Inc, Heidelberg Materials, and Boral, respectively, were utilized in the experiments. The chemical characteristics of the PC, slag, and fly ash as provided by the manufacturer are presented in Table 2. The mix designs of the slag pastes and fly ash pastes, and their designations are shown in Table 3. The control pastes of the slag paste and fly ash paste are designated as S and FA, respectively. S-HL-A, S-HL-B refer to the slag pastes containing HL-A and HL-B, respectively. Similarly, FA-HL-A, FA-HL-B refer to the fly ash pastes containing HL-A and HL-B, respectively. The percentage of slag and Fly ash in the S and FA pastes were 70 %. Control pastes without hydrogels were formulated with a water/binder (w/b) of 0.3. The hydrogel concentration used in the mixture was 1 % motivated by prior investigations indicating that this concentration is efficient for self-healing applications in cementitious materials [36,60,61]. To account for uptake of water by the hydrogels in the pastes containing hydrogels, the absorption values of the hydrogels are needed. Additional water is needed in the pastes containing hydrogels, due to the uptake of water by hydrogels, in order to keep the same effective water/binder in all pastes with and without hydrogels. To estimate the quantity of the additional water in the pastes containing hydrogels, water in small increments was added to these pastes and their flow measured until their flow values equal the flow value of the paste without hydrogels. This method of determining hydrogel absorption has been utilized in previous investigations [8,20,21,62].

The value of the flow test obtained for the pastes without hydrogels (control pastes) was measured to be 16 cm and 17 cm for slag and fly ash pastes, respectively. For the flow test, the fresh mixture was poured into a cone (height: 5 cm, bottom diameter: 7 cm and top diameter: 10 cm) and then allowed to rest on a table. After 5 min, the cone was lifted, and the table was dropped 25 times during a 15 second time period. The flow value was determined as the average of two diametrical dimensions of the spread. The flow test was conducted three times and averaged for each mixture. It is noted from the water/binder as listed in Table 3 that hydrogel HL-B demonstrated a higher water absorption compared to hydrogel HL-A. For pastes containing hydrogels, dry hydrogels were first

Table 3
Mix design and flow of the slag pastes and fly ash pastes.

Paste Designation	Water/Binder	Cement Replacement (%)	Superplasticizer (%)	Hydrogel (% binder mass)	Flow (cm)
S	0.3	70	0.167	-	16
S-HL-A	0.45	70	0.167	1	16
S-HL-B	0.55	70	0.167	1	16
FA	0.3	70	0.167	-	17
FA-HL-A	0.4	70	0.167	1	17
FA-HL-B	0.55	70	0.167	1	17

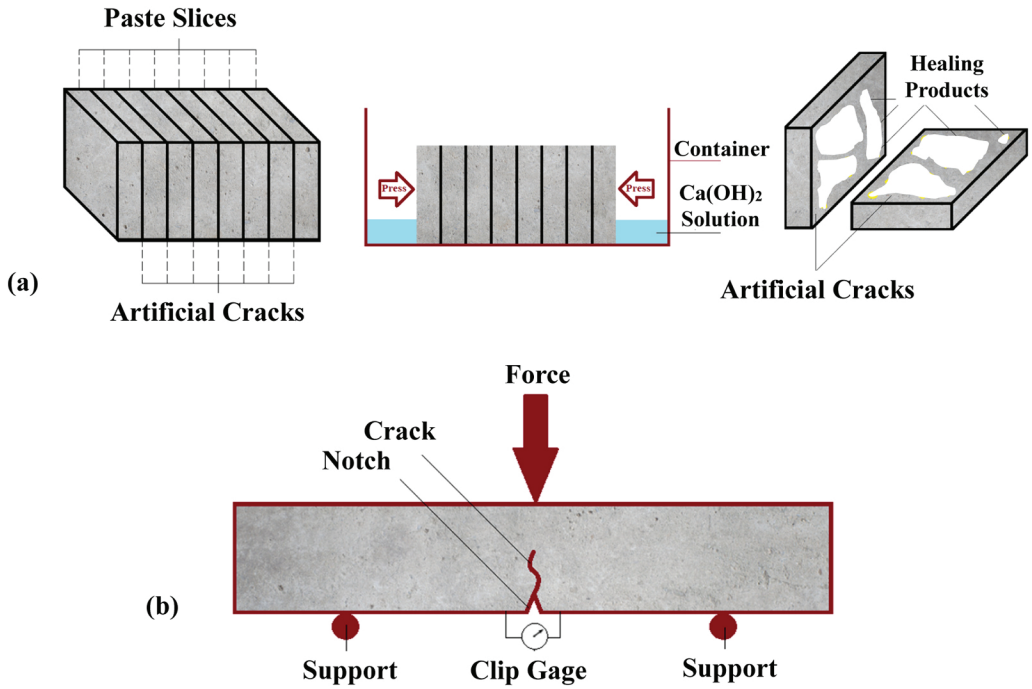

Fig. 1. Schematics of the samples used in (a) the characterization of the healing products and (b) mechanical regain experiments of the pastes.

dry mixed with binders for 5 minutes to ensure a homogenous dispersion of the hydrogels in the mixture. The mixtures were mixed in a bucket at a rate of 440 rpm for 30 seconds; then the inside wall of the bucket was scraped for 5 seconds, and then the mixture was mixed again for 60 seconds this time at a rate of 2600 rpm. The mixtures were cast into 50 mm × 50 mm × 50 mm plastic molds per the ASTM C 109. The mixtures were enveloped in a pre-stretched plastic wrap to inhibit moisture loss. After 24 hours, the cubes were demolded and sealed in polyethylene bags until the testing phase.

2.2. Methods

2.2.1. Microstructural and chemical characterization

2.2.1.1. Sample preparation. In order to obtain healing products (HP) in sufficient quantities needed in the microstructural and chemical characterization tests, including TGA, FTIR, SEM, and EDS, artificial paste cracks were prepared, as employed in previous studies [8,63]. Paste cubes were cut at the age of 28 days and slices in the dimensions of 50 mm × 50 mm × 15 mm were prepared (see Fig. 1a). The paste slices were then carefully polished with silicon carbide sandpapers (#320, 500, and 1200). The fine polishing was done using 1 μm diamond paste to obtain very smooth and similar surfaces for all slices. The lubricating fluid used during polishing was water. After vacuum drying the slices, they were then pressed against each other and placed partially in the curing solutions (see Fig. 1a). The slag paste slices were healed in saturated $Ca(OH)_2$ solution for 14 days, while the fly ash paste slices were healed in the $Ca(OH)_2$ solution with a pH >13. It is well known that slag is activated at a pH of about 12, whereas fly ash requires a pH exceeding 13 [17]. The pH of the healing solution for fly ash pastes was increased using sodium hydroxide. The pH of the saturated lime solution was measured to be 12.7. It should be noted that the healing solutions used here could differ from the practical conditions. However, these solutions were used to accelerate the reactivity of slag and fly ash in the respective solution. This allows us to focus our attention on the effect of hydrogels in the self-healing processes of slag and fly ash pastes. The gap between the slices, which serves as artificial cracks, was measured using an optical microscope to be approximately 42 μm. The lower portion of the slices were immersed in the solution. In this case, the solution was drawn into gaps through the capillary forces. Using this setup, the formed (HP) on the surfaces of the slices can be scraped with ease. The formed HP were then dried by vacuuming for 24 hours after being scratched off from the surfaces and used in microscopic and chemical characterizations.

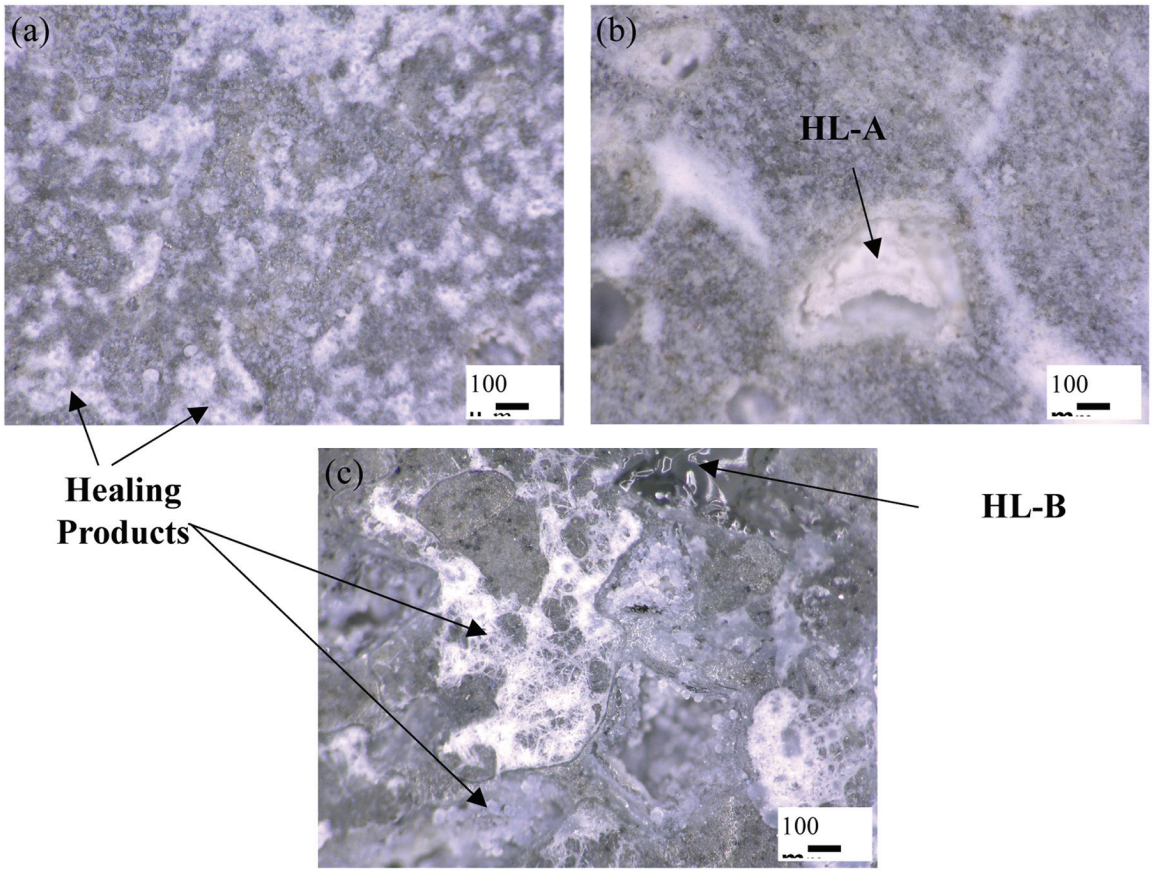

Fig. 2. Optical microscopic images of the healing products formed on the artificial crack surface of (a) S, (b) S-HL-A and (c) S-HL-B.

2.2.1.2. TGA. The TGA analysis was conducted in a TGA 55 TA Instrument under nitrogen gas. The data was collected between the temperatures of 25 °C and 1000 °C and at the rate of 10 °C/min. Eqs. 1 and 2 were used to calculate the content of calcium hydroxide (CH) and calcium carbonate (CC), respectively:

$$CH = \frac{74.1}{18}\frac{\overline{M}}{M} \tag{1}$$

$$CC = \frac{100}{44}\frac{\overline{M}}{M} \tag{2}$$

where $\overline{M}$ and M, are the change in mass attributed to the dehydration of calcium hydroxide or decarbonation of calcium carbonate, and the mass before heating, respectively.

2.2.1.3. FTIR. The FTIR analysis of the HP was performed utilizing a Perkin Elmer Paragon 1000 FTIR equipped with an ATR accessory. The scanning was conducted in the transmission mode with a resolution set at 4 cm^{-1} and within the range of 600 – 4000 cm^{-1}.

2.2.1.4. SEM/EDX. The microstructure of the HP was examined in a JEOL SEM/EDS. To prevent charging during SEM imaging, a nanolayer of gold was coated on the sample surface with a sputter coater. Imaging was conducted at an acceleration voltage of 15 kV and a magnification of 20 Kx. Elemental analysis was performed on several spots via EDS.

2.2.2. Mechanical regain and crack filling

The mechanical regain and crack filling abilities of hydrogels in the slag and fly ash pastes are examined in this study. of the pastes, paste prisms (2.54 cm × 2.54 cm × 15 cm) were cast (see Fig. 1b). The mix designs are the same as detailed in Table 3, but with a modification: PVA fibers with a diameter of 38 μm were incorporated at a volume percentage of 2 % into the specimens. This addition was to prevent failure during precrack generation and to enhance ductility. A rotating diamond blade was used to notch all specimens at their center. The notch was 2.0 mm wide and 1.5 mm deep. To induce precracks in the specimens, they were subjected to loading in a three-point bend setup at a rate of 2 $\times 10^{-4}$ mm per second using an Instron mechanical frame, and the crack opening was tracked with the aid of a clip gage, as depicted in Fig. 1b. The clip gage was employed to monitor the crack opening width. The loading ceased when the crack opening reached 0.2 mm, followed by unloading of the specimens. After complete unloading, the cracks were imaged via an optical microscope and the average crack width was approximately 60 μm.

After crack generation, the cracked specimens underwent dry-wet cycles for healing. Each dry/wet cycle consisted of a 1-hour wet period, during which the specimens were submerged in the same solution as those used for the paste samples used in the chemical and microstructural characterization, followed by 23 hours of being subjected to the ambient environment in the laboratory (relative humidity: 60 % and temperature: 23 °C). The healing was conducted for 28 days cycles, which was equivalent to 28 days. Following a period of 28 cycles of healing, the specimens were loaded until failure in the three-point bend setup. The regain in strength, called mechanical regain (MR), was calculated using Eq. 3:

$$MR\ (\%) = \frac{P_{max,healing} - P_{unloading}}{P_{max,initial} - P_{unloading}} \times 100 \tag{3}$$

where $P_{max,initial}$ represents the ultimate force obtained in the initial loading to induce the initial crack width, $P_{max,healing}$ denotes the ultimate force reached in the healed specimens, $P_{unloading}$ denotes the residual load. This residual load corresponds to the point where the

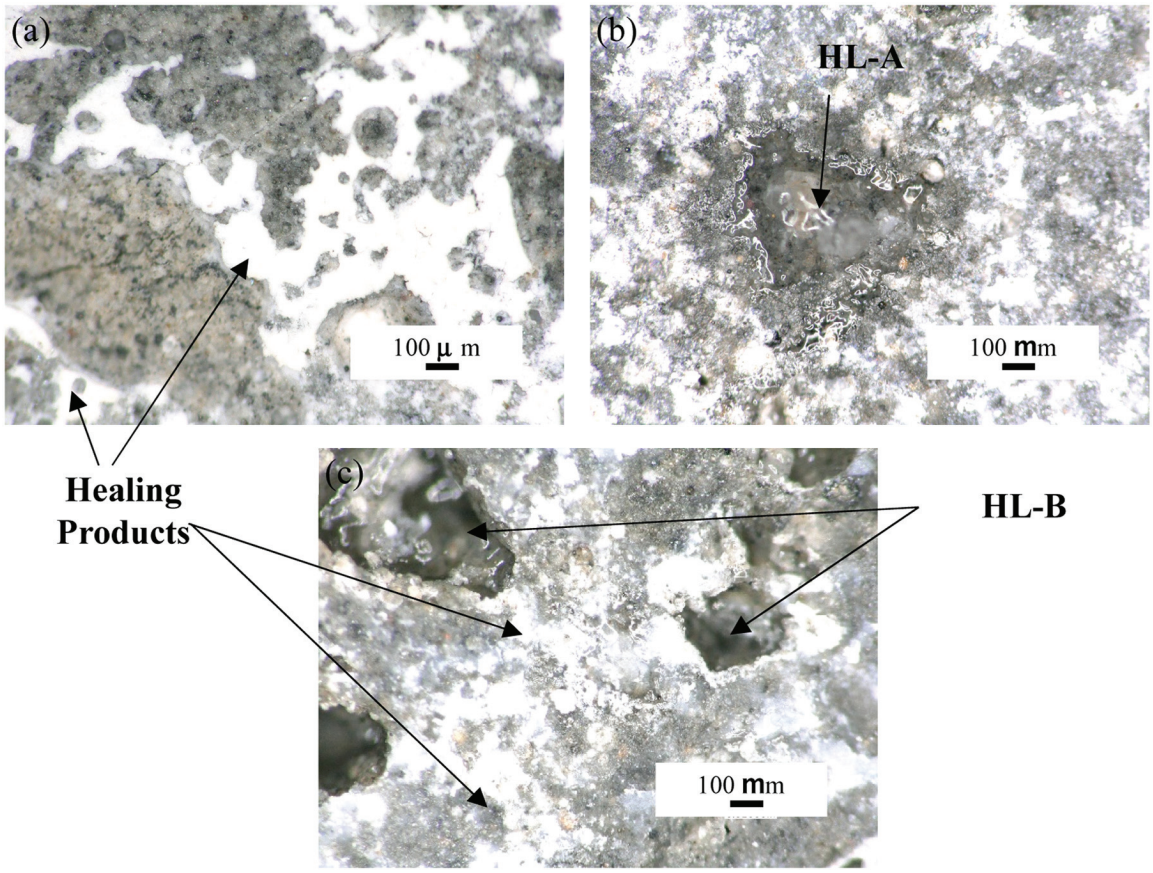

Fig. 3. Optical microscopic images of the HP formed on the artificial crack surface of (a) FA, (b) FA-HL-A and (c) FA-HL-B.

initially defined crack width was attained. A KEYENCE VHX 5000 optical microscope was used to monitor crack filling in the paste specimens. The images of the two sides of the specimens were taken after 3, 7, 14, and 28 cycles of healing.

3. Results and discussion

3.1. Characterization of the HP

3.1.1. Optical imaging

Fig. 2 shows the formation of the healing products (HP) on the surfaces of the artificial cracks in the control slag paste and slag paste with HL-A and HL-B. The HP appear as a white color substance partially covering the surface of the slag paste as seen in this figure. Fig. 3 shows the formation of the HP on the surfaces of the artificial cracks in fly ash pastes. The HP is seen as a whitish substance and seem to have a nonuniform coverage of the artificial crack surface. Hydrogels are marked on the crack surface.

3.1.2. TGA

Fig. 4a and b show, respectively, the mass loss and derivative mass loss profiles of the HP scratched from the surfaces of slag pastes as well as the bulk slag paste at the age of 28 days. After healing time of 14 days, the HP was scratched off from the slices and then dried by vacuuming for 24 hours. Mass loss in the temperature range of less than 200 °C is due to the evaporation of free water and water loss of ettringite [64,65] and C-S-H [64]. Small shoulders at 140 °C and 270 °C in the DTG curve of the HP are seen and are contributed to the decomposition of hemicarboaluminate [66] and monocarboaluminate [67]. There is a weak band at 430–450 °C in the DTG profiles of the bulk paste and to a lesser extent in the HP, which can be attributed to calcium hydroxide [68]. This calcium hydroxide comes about from the hydration of cement. A small peak at approximately 360 °C in the bulk paste is observed that is indicative of the presence of hydrotalcite [69]. The peak between 550 °C and 750 °C, observed in the DTG curves of the HP, can possibly be due to the decomposition of calcium carbonate [70,71]. This peak is noticeably small in the DTG curves of the bulk pastes. It should be noted that, according to [68], the decompositions of hemicarboaluminate and monocarboaluminate also occur in this range of temperature. Thus, a more detailed characterization investigation is needed to evaluate the percentage of each of these potential phases in the HP. The presence of CH, C-S-H, ettringite, AFm, and hydrotalcite was documented in slag-cement pastes [72–78].

The percentage of $CaCO_3$ content in the HP of the slag pastes are shown in Fig. 5. It is seen that the percentage of $CaCO_3$ in the HP of the paste containing HL-A and HL-B is higher than that of the control paste without hydrogel. No difference is observed in the percentage of $CaCO_3$ in the HP of the pastes containing HL-A and HL-B. It appears that the presence of hydrogels favored the precipitation of $CaCO_3$ over continued hydration in the crack in the slag pastes.

Fig. 6a and b show the mass loss and derivative mass loss profiles, respectively, of the HP and bulk paste of the fly ash pastes. Major peaks are noted in the derivative mass loss profile of HP. The mass loss occurring in the range of temperature less than 200 °C is attributed to the loss of free water and the dehydration of C-S-H and ettringite [79]. It is observed that the mass loss in the range of temperature less than 100 °C is notably lower in the case of HP compared to the bulk paste. Since ettringite decomposition starts at a temperature less than 100 °C and all samples underwent similar drying process during sample preparation, the small mass loss in the range of temperature less than 100 °C in HP indicates a very small presence of ettringite in the case of HP compared to the bulk paste of the fly ash pastes. According to the literature [80,

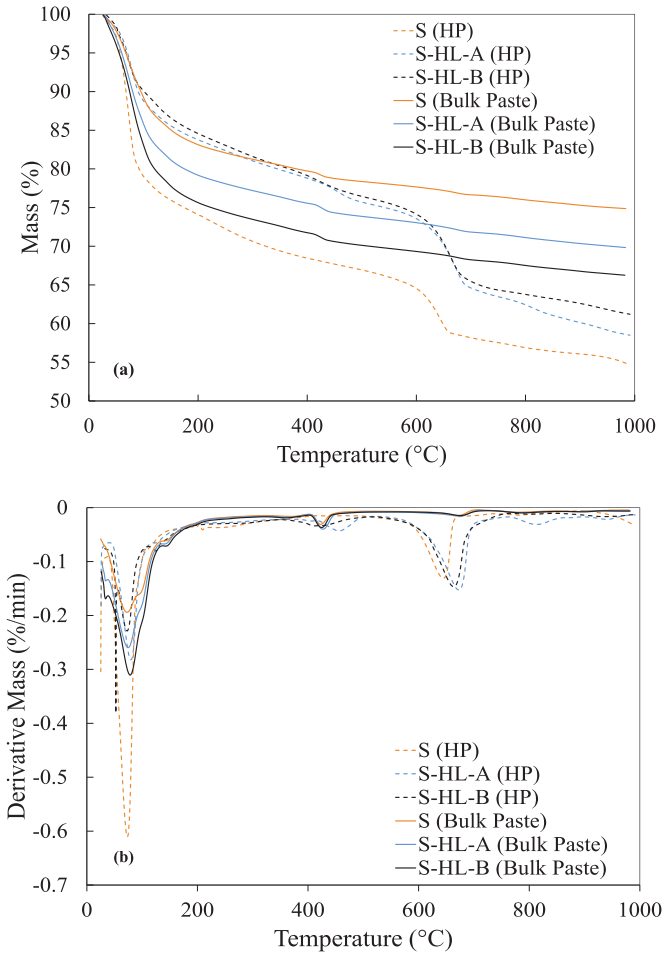

Fig. 4. (a) TG and (b) DTG curves of the HP and bulk pastes corresponding to slag pastes.

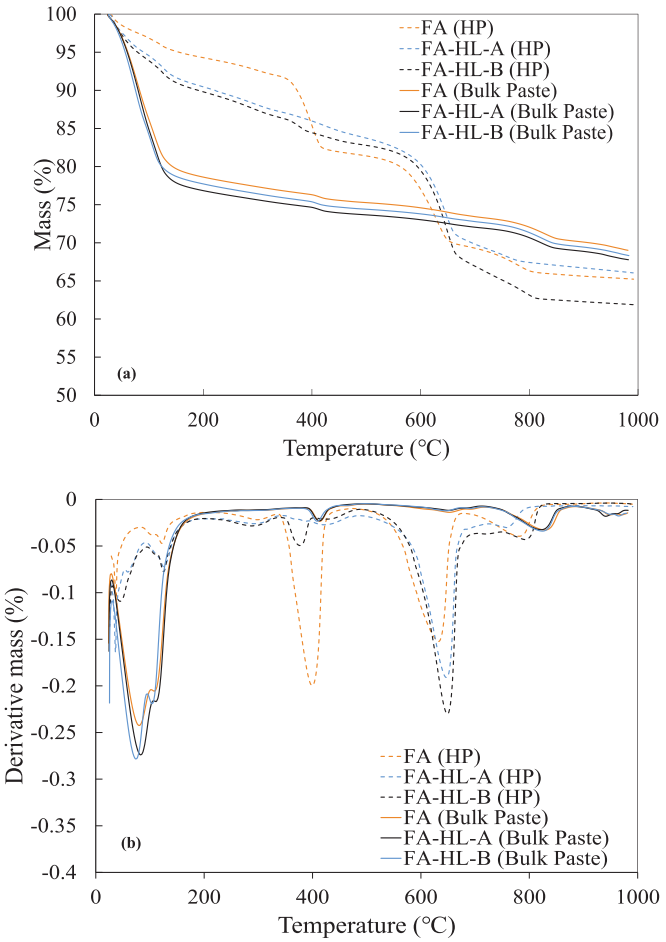

Fig. 6. (a) TG and (b) DTG curves of the HP and bulk pastes corresponding to fly ash pastes.

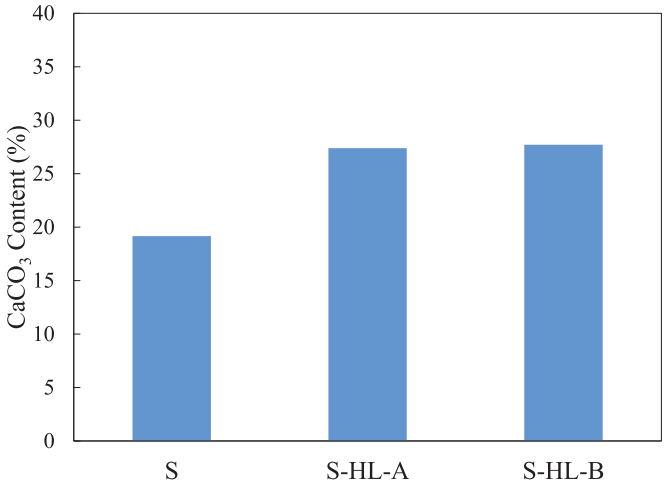

Fig. 5. $CaCO_3$ content in the HP of slag pastes.

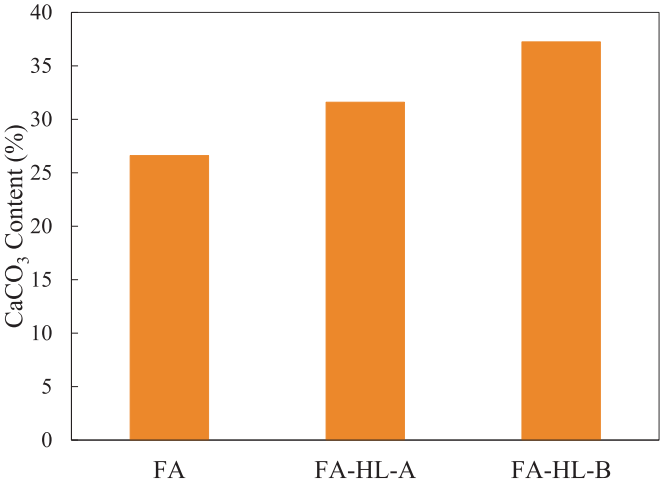

Fig. 7. $CaCO_3$ content in the HP of fly ash pastes.

81], in high content fly ash paste, calcium ion can combine with silicon and aluminum ions to form different forms of calcium-silicate-aluminate-hydrate (C-A-S-H) in small quantities. C-A-S-H has characteristics mass losses in the range of 415 – 430 °C and 649 – 660 °C [82]. In addition, $Ca(OH)_2$ has a mass loss peak in the range of 350 – 460 °C [83]. The FTIR results supported the presence of $Ca(OH)_2$ in HP. The occurrence of the characteristics peaks associated with $Ca(OH)_2$ and C-A-S-H in around a similar temperature range prevents an accurate quantification of these two phases in the HP. A large mass loss in the range of 350 – 460 °C in the HP of the control fly ash paste is noted; we believe this is an anomaly due to the uptake of $Ca(OH)_2$ from the healing solution. The significant mass loss noted in the range of 550 °C – 900 °C is associated with calcium carbonate [82,84].

The $CaCO_3$ content of the HP of the fly ash pastes is depicted in Fig. 7.

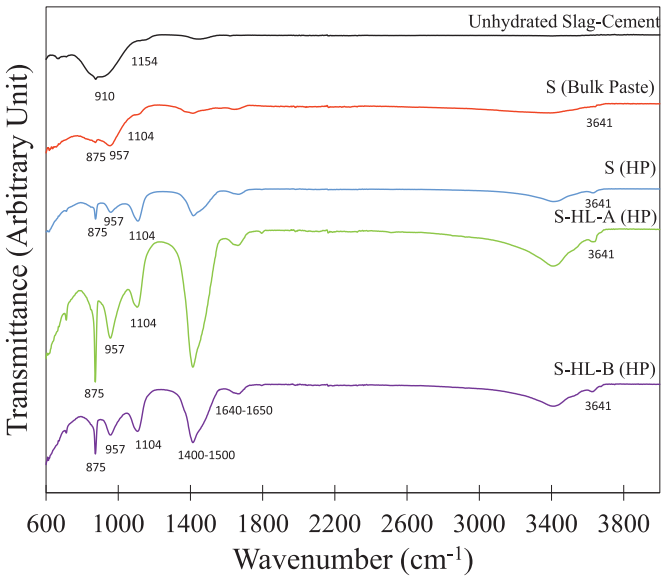

Fig. 8. FTIR spectra of the HP and bulk paste corresponding to slag pastes.

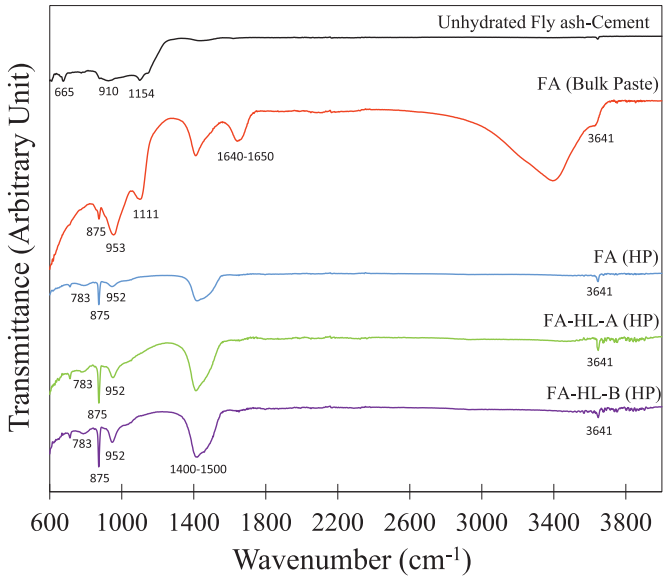

Fig. 9. FTIR spectra of the HP and bulk paste corresponding to fly ash pastes.

It is noticed that the HP of the fly ash with hydrogels have more $CaCO_3$ compared to the control fly ash paste without hydrogels. The increase in $CaCO_3$ formation in the case of the paste with hydrogels seems to be consistent with the observation made of the slag paste as shown in Fig. 4. It is noted that the HP of the fly ash pastes demonstrated a higher $CaCO_3$ compared to that of the slag pastes.

3.1.3. FTIR

The chemical characteristics of the HP scratched from the artificial cracks of the slag pastes were also evaluated via FTIR. As presented in Fig. 8, all the spectra of bulk slag paste and HP had bands in between 800 cm^{-1} and 1200 cm^{-1}, which are attributed to the stretching vibration of Si-O [85] or asymmetric stretching of SO_4^{2-} [86,87]. Due to the hydration of slag paste, the peak at 910 cm^{-1} in the spectrum of unhydrated slag shifted to 957 cm^{-1} in the profile of the bulk slag paste and HP, indicative of the presence of C-S-H gels [85,88]. The peak at 1104 cm^{-1} in the profiles of the bulk slag paste and more noticeably in the HP is due to SO_4^{2-} in ettringite [89,90]. The bands at approximately

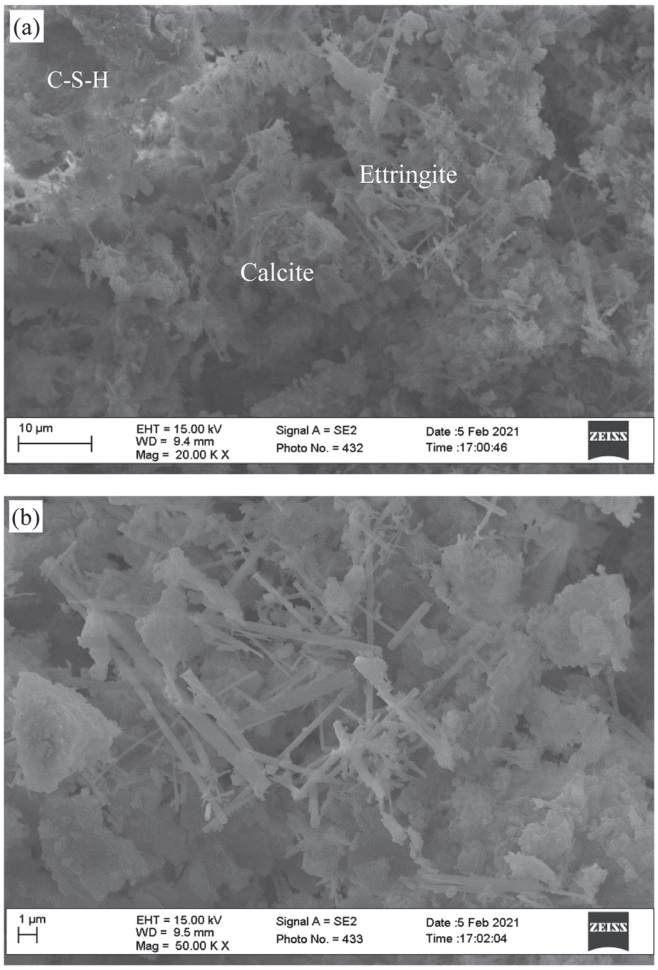

Fig. 10. (a) and (b) Micrographs showing the morphology at different magnifications of S-HP.

875 cm^{-1} and in between 1400 and 1500 cm^{-1} correspond to the out-of-plane bending [91,92] and the asymmetric stretching of CO_3^{2-} [93,94], respectively, which provides evidence for the formation of calcium carbonate. It is seen that these carbonate peaks are more pronounced in the HP of the paste with hydrogels, S-HL-A and S-HL-B, than in the control slag paste S. This observation corroborates the TGA observation discussed earlier regarding the calcium carbonate content in the pastes. The bands in 1640 −1650 cm^{-1} and 2800–3700 cm^{-1} are due to the presence of O-H in the bulk slag paste and HP [85]. The peaks at 1104 cm^{-1} and 1422 cm^{-1} in the profiles of HP appear stronger than those in the profile of the bulk slag paste. This provides evidence of the presence of more sulfate and carbonate phases in HP. Moreover, the peak at 3640 cm^{-1} indicates the presence of a small amount of $Ca(OH)_2$ in the HP [95].

The FTIR results of the HP of the fly ash pastes are shown in Fig. 9. Due to the pozzolanic reaction, the peak at approximately 910 cm^{-1} in the spectrum of the unhydrated cement fly ash shifted to 953 cm^{-1} in the case of the bulk fly ash paste, as shown in Fig. 9. The small shoulder in the spectrum of the HP and bulk paste at 783 cm^{-1} is attributed to the Al–OH bond in Al $(OH)_6$ of fly ash systems [96]. A peak at about 1111 cm^{-1} noted only in the profile of the bulk fly ash is attributed to SO_4^{2-} in ettringite [89,90]. This peak disappears in the profiles of the HP. This observation seems to agree with the TGA result discussed earlier indicating a very small amount of ettringite in the HP compared to the bulk paste of the fly ash pastes. The bands in the range of 1640 −1650 cm^{-1} and 2800–3700 cm^{-1} observed in the case of the bulk paste are typical for H-O-H vibrations [85] indicating the presence of free

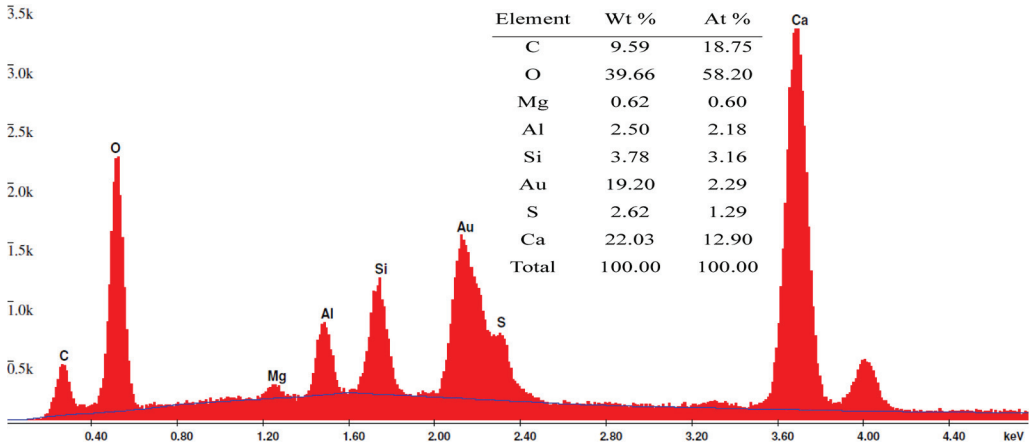

Fig. 11. EDS spectrum of the S-HP.

Table 4
Elemental ratio of the HP and bulk paste of slag pastes.

	S (HP)	S (Bulk Paste)
Ca/Si	3.9	1.9
Al/Si	0.67	0.4

water in the sample. These peaks are not evident in the case of HP despite using the same drying process for all samples. The C–O bending vibration at approximately 875 cm^{-1} and the broad band in between 1400 and 1500 cm^{-1} are the characteristic bands of CO_3^{2-} [85,97]. The peak noted at 3641 cm^{-1} is associated with the OH bond in $Ca(OH)_2$ [97]. The main peaks seem to occur at similar locations in the profiles of the HP and the bulk paste. However, these peaks show varied strength. The peaks at 783 cm^{-1} and 1400–1500 cm^{-1} in the profile of HP appear stronger than those in the profile of the bulk paste. This points to the presence of more aluminate and carbonate phases in the HP compared to the bulk paste.

3.1.4. SEM/EDS

The microstructure of the HP on the artificial cracks of the slag pastes was examined via scanning electron microscopy, as shown in Fig. 10. Different morphologies were found in HP of the slag pastes. The needle-like morphology is attributed to ettringite [98]. EDS shows sulfur in the spectrum, which is indicative of the presence of ettringite in the HP. A gel-like morphology can be seen in the micrograph of the HP, which is attributed to C-S-H gel [99]. Moreover, crystal-like features are seen in the image, which could be primarily calcium carbonate. This seems to be consistent with the results obtained from TGA and FTIR that showed C-S-H, ettringite, and $CaCO_3$ are formed in the HP.

The chemical elements of the HP shown in Fig. 11 were analyzed by EDS. Carbon, oxygen, magnesium, aluminum, silicon, sulfur, and calcium are the elements that are detected by EDS in the HP of the slag paste. The Ca/Si and Al/Si of the bulk paste and HP of slag pastes are shown in Table 4. The large percentage of C and Ca in the elemental analysis is an indicative of $CaCO_3$ being a primary phase in the HP. $CaCO_3$ is precipitated as a result of the reaction between Ca^{2+} and CO_3^{2-} ions when CO_2 is present in the crack [100]. The presence of CO_3^{2-} was also detected by FTIR. The Ca^{2+} ions exist in the solution since the slice were cured in saturated $Ca(OH)_2$, as mentioned earlier. Sulfur is detected in the spectra indicating the presence of the ettringite. It is noticed that FTIR confirmed the presence sulfate phases in HP. Besides FTIR, SEM confirmed the existence of ettringite. The higher Ca/Si and Al/Si of the HP compared to the bulk slag paste as seen in Table 4 is an indication of higher content of carbonate and aluminate containing phases in the HP. The SEM imaging and EDS analysis of the HP of pastes with and without hydrogels showed similar behaviors, so only the results of the control slag paste are included here.

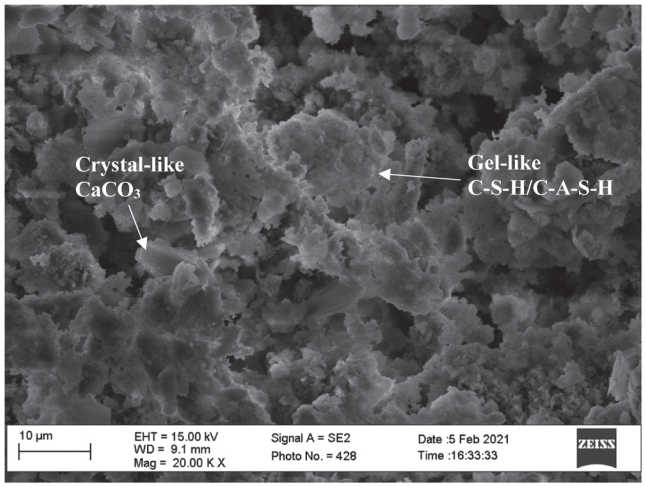

Fig. 12. SEM micrograph of the HP of FA.

The composition of the phases in the HP can help in understanding the underlying mechanisms involved in self-healing. It is well known that slag is a pozzolan that can be activated by alkalis [101,102]. A pH of 12 was reported to be adequate to trigger activation of slag [103]. In this study the slag paste slices at the age of 28 were cured in saturated $Ca(OH)_2$ solution. Unhydrated slag particles are available on the surfaces of the artificial cracks. Once they are exposed to the saturated $Ca(OH)_2$ solution, they begin releasing ions including Ca^{2+}, OH^-, SiO_2(aq), Al^{3+}, Mg^{2+}, S, etc into the solution in the crack, leading to an increase in the ionic concentrations in the crack. This increase in the ionic concentrations causes supersaturation, leading to the formation of various phases in the HP.

Moreover, due to the gradients of ion concentrations, ion exchange takes place between the solution in cracks and the pore solution in the bulk paste. The concentrations of Ca^{2+} and OH^- are almost 2.1 mM and 15 mM in slag paste at 28 days [64], while the concentrations of Ca^{2+} and OH^- are 22.4 mM and 44.8 mM in saturated $Ca(OH)_2$ solution. Therefore, these concentrations of Ca^{2+} and OH^- are lower in the bulk paste than in the saturated $Ca(OH)_2$ solution. Thus, Ca^{2+} and OH^- diffusion occurs from the cracks towards the interior bulk material; on the other hand, other ions diffuse from the interior bulk material towards cracks. The saturation criterion is easier to reach for the phases with a lower solubility. Therefore, it takes more time for ions in slag paste to diffuse into the solution. Thus, low soluble phases such as C-S-H

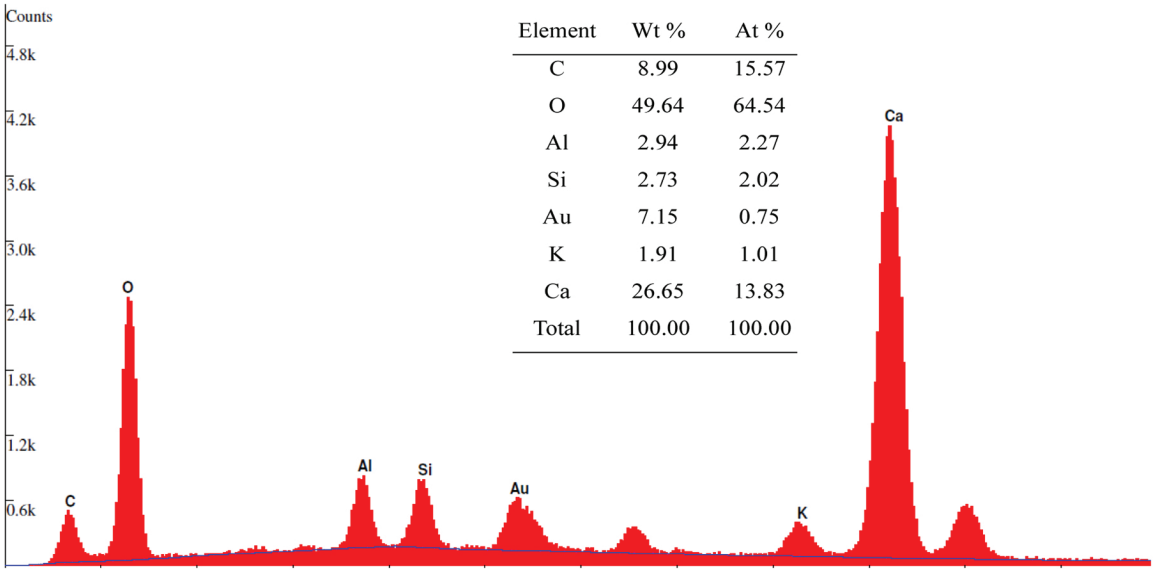

Element	Wt %	At %
C	8.99	15.57
O	49.64	64.54
Al	2.94	2.27
Si	2.73	2.02
Au	7.15	0.75
K	1.91	1.01
Ca	26.65	13.83
Total	100.00	100.00

Fig. 13. EDS spectrum of the HP of FA.

Table 5
Elemental ratio of the HP and bulk paste of fly ash pastes.

	FA (HP)	FA (Bulk Paste)
Ca/Si	6.3	1.2
Al/Si	1	0.5

and hydrotalcite are favored to precipitate in the vicinity of unhydrated slag particles.

Fig. 12 shows the micrograph of the HP of the fly ash paste. Both crystal-like and gel-like microstructure be noted in the microstructure. The crystal-like morphology is most likely attributed to calcium carbonate phase, which was shown by TGA to be present in the healing product. The gel-like morphology is attributed to be C-S-H or C-A-S-H.

The chemical elements of the HP are shown in Fig. 13. The major elements in the HP of the fly ash paste are Ca, Si, Al, and O. The Ca/Si and Al/Si of the HP are provided in Table 5. It is noted that the Ca/Si and Al/Si of the HP of the fly ash paste with a mean value of 6.3 and 1, respectively, are larger than in the bulk fly ash paste with the mean values of 1.2 and 0.5 respectively. This indicates the presence of more calcium carbonate and aluminate-rich compounds in the HP than in the bulk paste. The SEM imaging and EDS analysis of the HP of the pastes with and without hydrogels showed similar behaviors, so only the results of the control fly ash paste are included here.

3.2. Mechanical regain

A primary purpose of self-healing is the regain in strength of the cementitious materials. To evaluate mechanical regain, prism specimens ($2.54 \times 2.54 \times 15\ cm^3$) were notched and precracked employing the setup shown in Fig. 1b. The crack width and length in the specimens were measured by an optical microscope and the average of 60 ± 6 μm and 7 ± 0.22 mm, respectively, was obtained. The specimens were then subjected to the wet/dry cycles (1 hour in solution and 23 hours in the ambient environment in the laboratory with relative humidity of 60 % and temperature of 23 °C) for 28 days in two different solutions, deionized water and saturated lime solutions.

With respect to the specimens that were healed in deionized water, no crack filling was observed over the period of 28 days. This is primarily due to the lack of $Ca(OH)_2$ in the paste. It should be mentioned that the replacement of the supplementary cementitious materials in this study is 70 % (70 % SCM and 30 % OPC) and the specimens were prepared at the age of 28 days; therefore, a high percentage of $Ca(OH)_2$ was used up in the specimens due to the pozzolanic activity. The presence of $Ca(OH)_2$ is required for continued hydration of SCM during the healing process as well as crystallization of $CaCO_3$ when CO_2 is

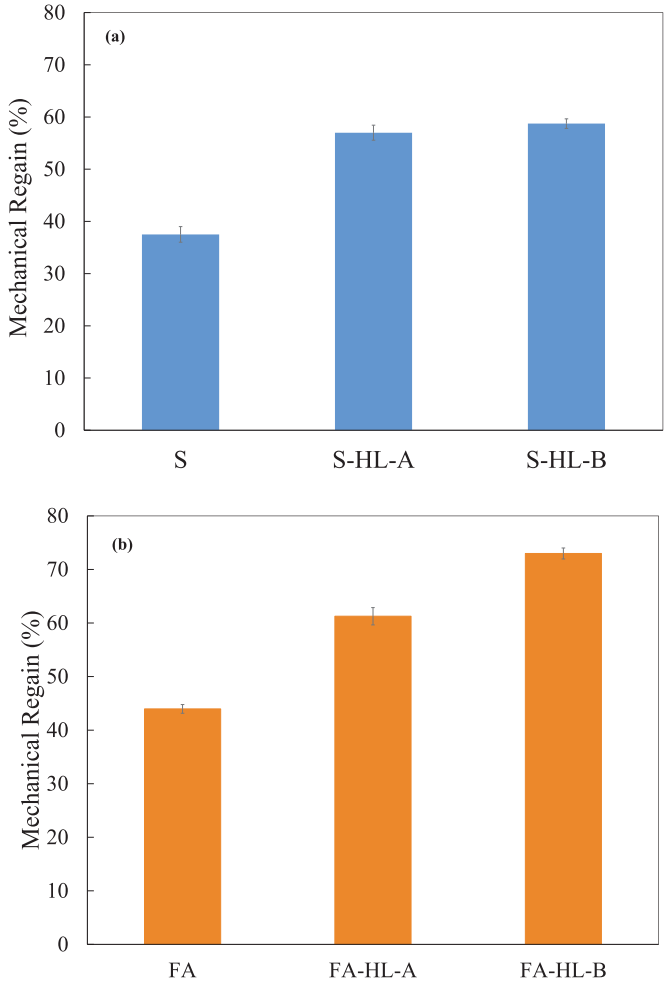

Fig. 14. Mechanical regain of cracked (a) slag pastes and (b) fly ash pastes.

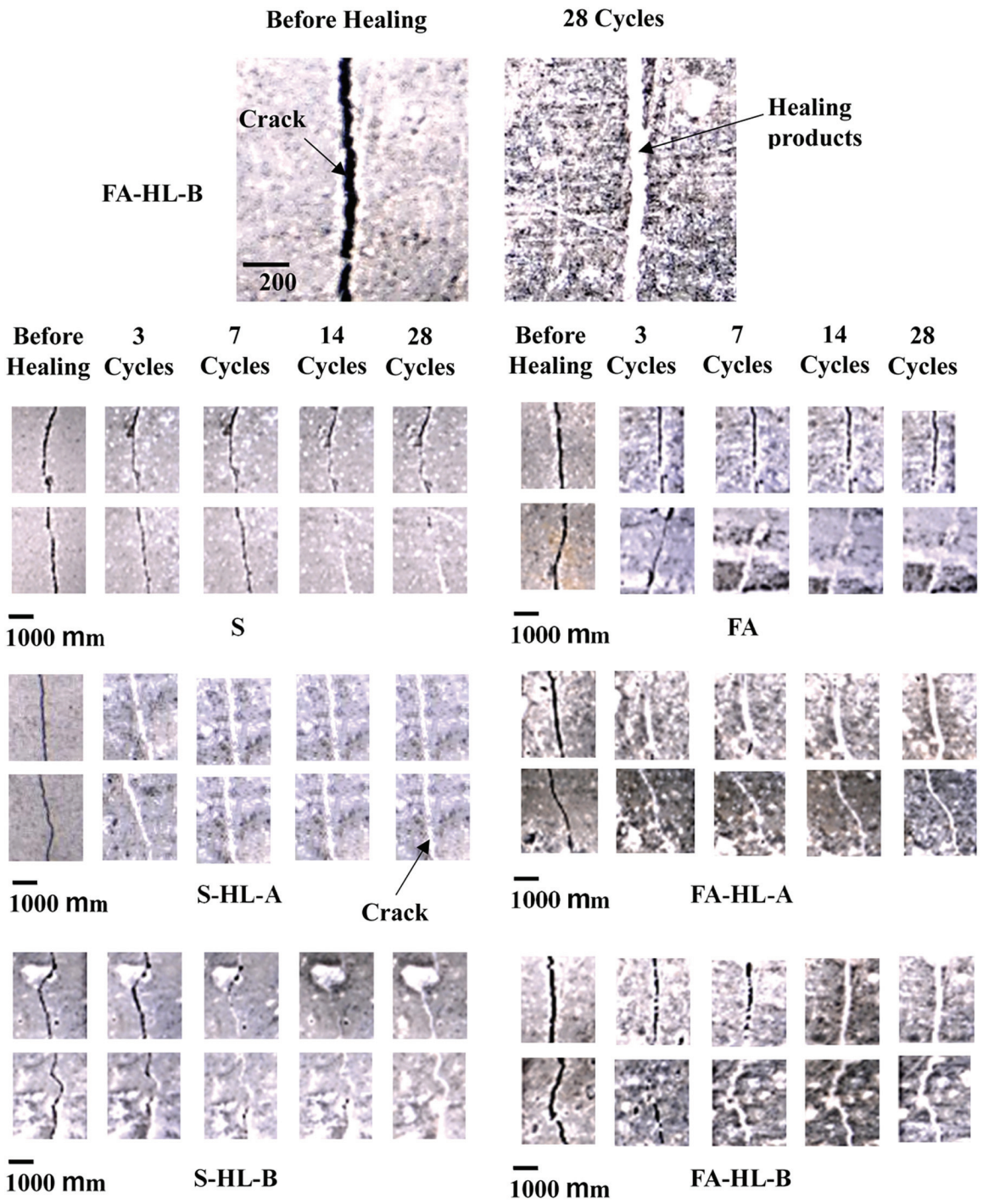

Fig. 15. Optical images showing the crack filling evolution of the cracked pastes.

available, which is the case in cracks [68]. In high dosage supplementary cementitious materials (SCM), $Ca(OH)_2$ is not available in sufficient amount for further reaction of SCM and $CaCO_3$ crystallization. The CH content, measured from the TGA results, in the bulk slag paste and fly ash paste at 28 days was in the range of 4–5 % and 3–4 %, respectively, indicating very low CH content in these pastes. The CH contents agrees well with the literature [104]. A CH content of slightly more than 4 % was reported by [104] in slag paste with slag dosage of 70 %. In contrast to the specimens healed in deionized water, the specimens healed in saturated lime solution demonstrate crack filling within the first 5 dry/wet cycles. As discussed in Section 3.1.1. and 3.1.2., $CaCO_3$ and hydration products, including C-S-H gel and ettringite, were shown to be the primary HP in the case of the slag pastes. As mentioned previously, in this study the slag paste specimens were immersed in the saturated $Ca(OH)_2$ solution for one hour every 24 hours during the dry/wet cycle. The $Ca(OH)_2$ was utilized to trigger activation of unreacted slag on the crack surface. The C-S-H gel is formed through the pozzolanic reactions and exists primarily near the unreacted slag on the surface of microcracks.

Fig. 14a shows the mechanical regain of the slag paste specimens. The control specimen without hydrogels showed about 37 % mechanical regain. The slag paste specimens with HL-A and HL-B exhibited a higher mechanical regain (57 % and 59 %, respectively) than the control specimen. A slightly higher mechanical regain in the specimen with HL-

B than the specimen with HL-A can be noted.

The dosage of the hydrogel used in this study is 1 % of the binder; therefore, when cracks arise, hydrogels are more likely to be present on the crack path as hydrogel macrovoids create regions of high stress concentration at the microscale. When the external fluid comes into contact with hydrogels on the crack surfaces in the wet period, hydrogels swell, physically blocking the crack. During the dry period, hydrogels release their water into the crack space, stimulating healing. The higher absorption of HL-B than HL-A and as such, availability of more water during the dry cycle, could promote an increase in the formation of healing product in between cracks leading to higher mechanical regain.

The mechanical regain of the fly ash paste specimens is shown in Fig. 14b. Fly ash paste specimens demonstrated crack filling within the first few cycles, which is primarily attributed to $CaCO_3$ precipitation [105]. As discussed earlier, $CaCO_3$ is one of the major phases in the HP of fly ash pastes. The fly ash control paste specimen without hydrogels showed a mechanical regain of about 43 %. The fly ash pastes with HL-A and HL-B showed a higher mechanical regain of 61 % and 72 %, respectively, compared to the fly ash paste without hydrogels. A higher mechanical regain in the paste containing hydrogels than the paste without hydrogels is noted, which could point to the increased healing product when hydrogels are used in the fly ash pastes. A higher mechanical regain of the fly ash paste with HL-B compared to the fly ash paste with HL-A is observed. This trend agrees with the mechanical regain results of slag pastes, where HL-B appeared to have a larger effect than HL-A on increasing the mechanical regain of the samples.

The mechanical regain results presented above clearly provide evidence for the beneficial effect of hydrogels on the mechanical regain of slag and fly ash pastes. The impact of the chemical composition of the hydrogels on how they improve the mechanical regain could be different in different pastes; however, a general trend emerges that relates the effect on mechanical regain to the absorption capacity of the hydrogels. As shown previously, HL-B demonstrated a higher absorption behavior than HL-A; thus, HL-B can take up more water during the wet cycle and release a larger amount of water than HL-A during the dry cycle to promote formation of more HP. It should be borne in mind that availability of water is critical for the continued hydration and $CaCO_3$ formation.

3.3. Crack filling evolution

The filling of cracks was monitored as discussed in section 2.3. Fig. 15 shows the filling of the crack in the slag paste without hydrogels (S), and the slag pastes containing hydrogels (S-HL-A, and S-HL-B) before healing and at 3, 7, 14, and 28 cycles of healing. The optical images have been enhanced to allow visual observation of the filling of the crack with the healing products. The HP in the form of a whitish substance is seen to fill the crack in the specimen. During the crack filling evolution monitoring, it was observed that the cracks were filled by the HP on both sides of the prisms. Crack filling by formation of the HP appears to start within the first few cycles in the slag pastes containing HL-A and HL-B. As can be seen, the control slag paste without hydrogel showed formation of the HP at a later age of cycle 14. The crack in the slag pastes containing hydrogels were filled with the HP after healing for 28 cycles (days). But the slag paste without hydrogels showed only partial crack filling by this age. In the case of S-HL-A, the entire crack appears to be filled after 7 cycles. Although a large portion of the cracks was filled in S-HL-B at cycle 7, S-HL-B demonstrated a complete crack filling at cycle 14.

In the control fly ash paste (FA), the crack filling started after 7 cycles, while fly ash pastes containing HL-A and HL-B (FA-HL-A and FA-HL-B) demonstrated crack filling at the third cycle. The crack was entirely filled after 14 cycles in FA-HL-A and FA-HL-B, while the crack in FA was not entirely filled by HP even at 28 cycles.

As discussed previously, since hydrogels promote a preferential pathway for cracks, they are present on the crack surface. Due to their high water absorption and retention capacity, they are able to capture water during the wet cycle or from the humidity of the environment. During the dry cycle, the absorbed water is released from the hydrogels into the surrounding region (see Fig. 16). Since water plays an essential role in the chemical reactions underlying the precipitation of healing products, the provision of water from hydrogels can enhance the precipitation of the healing products thereby contributing to the crack filling in both slag and fly ash pastes. The crack filling evolution observations are in support of the mechanical regain results discussed earlier.

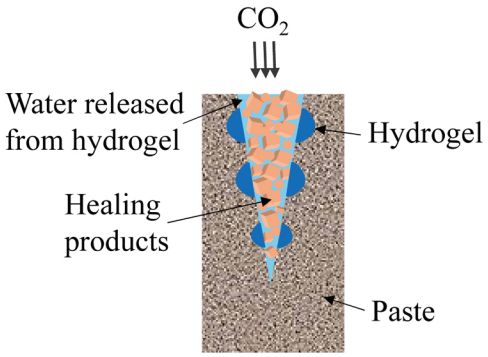

Fig. 16. Illustration depicting the effect of hydrogels on self-healing.

4. Conclusion

The influence of hydrogels on the self-healing processes in cementitious systems with a large dosage of slag and fly ash was studied. The conclusions are as follows:

- In the slag pastes, the HP were primarily made up of $CaCO_3$ and hydration product including C-S-H and ettringite. Other phases, including monocarboaluminate and hemicarboaluminate, were also observed in the healing product.
- The presence of C-S-H, C-A-S-H, and $CaCO_3$ phases was evidenced in the HP of the fly ash pastes. It was observed that the ratio of $CaCO_3$ to hydration products was larger in the case of fly ash paste than slag pastes.
- In both slag and fly ash pastes, the pastes with hydrogels demonstrated a higher $CaCO_3$ content than the control paste without hydrogels.
- A higher mechanical regain and crack filling in the pastes containing hydrogels than the paste without hydrogels is noted, which points to the increased healing product when hydrogels are used in the slag and fly ash pastes.
- The hydrogel with a higher water absorption generally seemed to exhibit a slightly improved impact on the mechanical regain and crack filling in both fly ash and slag pastes. However, further investigations can help in establishing the relationship between the hydrogel characteristics and their self-healing effect in systems containing slag and fly ash.

CRediT authorship contribution statement

Babak Vafaei: Writing – review & editing, Writing – original draft, Methodology, Data curation. **Ali Ghahremaninezhad:** Writing – review & editing, Writing – original draft, Investigation, Funding acquisition, Formal analysis, Conceptualization.

Declaration of Competing Interest

The authors declare that they have no known competing financial

interests or personal relationships that could have appeared to influence the work reported in this paper.

Data availability

Data will be made available on request.

Acknowledgement

This study was performed at the Advanced Infrastructure Materials Research Laboratory at the University of Miami and was supported by the National Science Foundation under the CAREER award number 1846984. Any opinions, findings, and conclusions or recommendations expressed in this material are those of the authors and do not necessarily reflect the views of the National Science Foundation.

References

[1] C.A. Hendriks, E. Worrell, D. De Jager, K. Blok, P. Riemer, Emission Reduction of Greenhouse Gases from the Cement Industry, n.d. ⟨http://www.ieagreen.org.uk/prghgt42.htm⟩.
[2] E. Worrell, L. Price, N. Martin, C. Hendriks, L.O. Meida, Carbon dioxide emissions from the global cement industry, Annu. Rev. Energy Environ. 26 (2001) 303–329, https://doi.org/10.1146/annurev.energy.26.1.303.
[3] B. Vafaei, K. Farzanian, A. Ghahremaninezhad, The influence of superabsorbent polymer on the properties of alkali-activated slag pastes, Constr. Build. Mater. 236 (2020) 117525, https://doi.org/10.1016/j.conbuildmat.2019.117525.
[4] M. Levine, M. Hirose, Energy Efficiency Improvement Utilising High Technology: An Assessment Of Energy Use In Industry And Buildings. Report and Case Studies, World Energy Council, London, 1995, pp. 46–150.
[5] J.G.J. Olivier, K.M. Schure, J. Peters, Trends in global CO2 and total greenhouse gas 2017 report, PBL Neth. Environ. Assess. Agency (2017).
[6] J.S. Damtoft, J. Lukasik, D. Herfort, D. Sorrentino, E.M. Gartner, Sustainable development and climate change initiatives, Cem. Concr. Res. 38 (2008) 115–127, https://doi.org/10.1016/j.cemconres.2007.09.008.
[7] U.S. energy-related carbon dioxide emissions fell in 2019, mainly in electric generation - today in Energy - U.S. Energy Information Administration, (EIA) (2021)., (n.d.).
[8] B. Vafaei, A. Ghahremaninezhad, Investigating the effect of hydrogel characteristics on the self-healing of cementitious materials, Mater. Struct. Mater. Et. Constr. 56 (2023), https://doi.org/10.1617/s11527-023-02265-y.
[9] F. Pacheco-Torgal, Z. Abdollahnejad, S. Miraldo, S. Baklouti, Y. Ding, An overview on the potential of geopolymers for concrete infrastructure rehabilitation, Constr. Build. Mater. 36 (2012) 1053–1058, https://doi.org/10.1016/j.conbuildmat.2012.07.003.
[10] Association, P.C. United States Cement Industry; Portland Cement Association: Skokie, IL, USA, 2016., (n.d.).
[11] B. Lothenbach, G. le Saout, M. ben Haha, R. Figi, E. Wieland, Hydration of a low-alkali CEM III/B–SiO2 cement (LAC), Cem. Concr. Res 42 (2012) 410–423.
[12] S. Qian, J. Zhou, M.R. De Rooij, E. Schlangen, G. Ye, K. Van Breugel, Self-healing behavior of strain hardening cementitious composites incorporating local waste materials, Cem. Concr. Compos 31 (2009) 613–621.
[13] D. Snoeck, J. Dewanckele, V. Cnudde, N. De Belie, X-ray computed microtomography to study autogenous healing of cementitious materials promoted by superabsorbent polymers, Cem. Concr. Compos 65 (2016) 83–93.
[14] S.Z. Qian, J. Zhou, E. Schlangen, Influence of curing condition and precracking time on the self-healing behavior of engineered cementitious composites, Cem. Concr. Compos 32 (2010) 686–693.
[15] M. Sahmaran, G. Yildirim, T.K. Erdem, Self-healing capability of cementitious composites incorporating different supplementary cementitious materials, Cem. Concr. Compos 35 (2013) 89–101.
[16] K. Van Tittelboom, E. Gruyaert, H. Rahier, N. De Belie, Influence of mix composition on the extent of autogenous crack healing by continued hydration or calcium carbonate formation, Constr. Build. Mater. 37 (2012) 349–359, https://doi.org/10.1016/j.conbuildmat.2012.07.026.
[17] J. Bijen, Benefits of slag and fly ash, Constr. Build. Mater. 10 (1996) 309–314, https://doi.org/10.1016/0950-0618(95)00014-3.
[18] H. Wang, M. Habibi, R. Marzouki, A. Majdi, M. Shariati, N. Denic, A. Zakić, M. Khorami, M.A. Khadimallah, A.A.K. Ebid, Improving the self-healing of cementitious materials with a hydrogel system, Gels 8 (2022), https://doi.org/10.3390/gels8050278.
[19] B. Vafaei, Prop. Self Heal. Cem. Mater. Hydrogel (2021).
[20] K. Farzanian, B. Vafaei, A. Ghahremaninezhad, The influence of the chemical composition of hydrogels on their behavior in cementitious materials, Mater. Struct. 54 (2021), https://doi.org/10.1617/s11527-021-01838-z.
[21] B. Vafaei, K. Farzanian, A. Ghahremaninezhad, Effect of Hydrogels Containing Nanosilica on the Properties of Cement Pastes, (2021) 1–19.
[22] M.J. Zohuriaan-Mehr, H. Omidian, S. Doroudiani, K. Kabiri, Advances in non-hygienic applications of superabsorbent hydrogel materials, J. Mater. Sci. 45 (2010) 5711–5735, https://doi.org/10.1007/s10853-010-4780-1.
[23] D. Kim, K. Park, Swelling and mechanical properties of superporous hydrogels of poly(acrylamide-co-acrylic acid)/polyethylenimine interpenetrating polymer networks, Polym. 45 (2004) 189–196, https://doi.org/10.1016/j.polymer.2003.10.047.
[24] S.G. Abd Alla, M. Sen, A.W.M. El-Naggar, Swelling and mechanical properties of superabsorbent hydrogels based on Tara gum/acrylic acid synthesized by gamma radiation, Carbohydr. Polym. 89 (2012) 478–485, https://doi.org/10.1016/j.carbpol.2012.03.031.
[25] E. Baffoe, A. Ghahremaninezhad, Effect of hydrogel on mitigating drying shrinkage induced cracking in carbonation cured calcium silicate binders, Constr. Build. Mater. 411 (2024) 134243, https://doi.org/10.1016/j.conbuildmat.2023.134243.
[26] L.P. Esteves, Superabsorbent polymers: On their interaction with water and pore fluid, Cem. Concr. Compos 33 (2011) 717–724.
[27] K. Farzanian, B. Vafaei, A. Ghahremaninezhad, The behavior of superabsorbent polymers (SAPs) in cement mixtures with glass powders as supplementary cementitious materials, Materials 12 (2019), https://doi.org/10.3390/ma12213597.
[28] J. Prabahar, B. Vafaei, A. Ghahremaninezhad, The Effect of hydrogels with different chemical compositions on the behavior of alkali-activated slag pastes, Gels 8 (2022) 731, https://doi.org/10.3390/gels8110731.
[29] Z. Li, S. Zhang, X. Liang, J. Granja, M. Azenha, G. Ye, Internal curing of alkali-activated slag-fly ash paste with superabsorbent polymers, Constr. Build. Mater. 263 (2020) 120985, https://doi.org/10.1016/j.conbuildmat.2020.120985.
[30] Z. Li, M. Wyrzykowski, H. Dong, J. Granja, M. Azenha, P. Lura, G. Ye, Internal curing by superabsorbent polymers in alkali-activated slag, Cem. Concr. Res. 135 (2020), https://doi.org/10.1016/j.cemconres.2020.106123.
[31] Z. Yang, P. Shi, Y. Zhang, Z. Li, Effect of superabsorbent polymer introduction on properties of alkali-activated slag mortar, Constr. Build. Mater. 340 (2022) 127541, https://doi.org/10.1016/j.conbuildmat.2022.127541.
[32] Z. Yang, P. Shi, Y. Zhang, Z. Li, Influence of liquid-binder ratio on the performance of alkali-activated slag mortar with superabsorbent polymer, J. Build. Eng. 48 (2022) 103934, https://doi.org/10.1016/j.jobe.2021.103934.
[33] J. Yang, Z. Sun, N. De Belie, D. Snoeck, Internal curing and its application to alkali-activated materials: a literature review, Cem. Concr. Compos 145 (2024) 105360, https://doi.org/10.1016/j.cemconcomp.2023.105360.
[34] S. Mönnig, P. Lura, Superabsorbent polymers—An additive to increase the freeze-thaw resistance of high strength concrete, in: Advances in Construction Materials 2007, Springer, 2007, pp. 351–358.
[35] V. Mechtcherine, C. Schröfl, M. Wyrzykowski, M. Gorges, P. Lura, D. Cusson, J. Margeson, N. De Belie, D. Snoeck, K. Ichimiya, Effect of superabsorbent polymers (SAP) on the freeze–thaw resistance of concrete: results of a RILEM interlaboratory study, Mater. Struct. 50 (2017) 1–19.
[36] D. Snoeck, S. Steuperaert, K. van Tittelboom, P. Dubruel, N. de Belie, Visualization of water penetration in cementitious materials with superabsorbent polymers by means of neutron radiography, Cem. Concr. Res. 42 (2012) 1113–1121.
[37] D. Snoeck, K. Van Tittelboom, N. De Belie, S. Steuperaert, P. Dubruel, The use of superabsorbent polymers as a crack sealing and crack healing mechanism in cementitious materials, Proc. 3rd Int. Conf. Concr. Repair, Rehabil. Retrofit. Cape Town South Afr. (2012).
[38] H.X.D. Lee, H.S. Wong, N. Buenfeld, Self-sealing cement-based materials using superabsorbent polymers, Proc. Int. RILEM Conf. Use Superabsorbent Polym. Other N. Addit. Concr., Lyngby, Den. (2010) 15–18.
[39] H.X.D. Lee, H.S. Wong, N.R. Buenfeld, Potential of superabsorbent polymer for self-sealing cracks in concrete, Adv. Appl. Ceram. 109 (2010) 296–302.
[40] D. Snoeck, N. De Belie, Repeated autogenous healing in strain-hardening cementitious composites by using superabsorbent polymers, J. Mater. Civ. Eng. 28 (2016) 04015086.
[41] D. Snoeck, K. Van Tittelboom, S. Steuperaert, P. Dubruel, N. De Belie, Self-healing cementitious materials by the combination of microfibres and superabsorbent polymers, J. Intell. Mater. Syst. Struct. 25 (2014) 13–24.
[42] H. Huang, G. Ye, C. Qian, E. Schlangen, Self-healing in cementitious materials: Materials, methods and service conditions, Mater. Des. 92 (2016) 499–511, https://doi.org/10.1016/j.matdes.2015.12.091.
[43] D. Snoeck, K. Van Tittelboom, S. Steuperaert, P. Dubruel, N. De Belie, Self-healing cementitious materials by the combination of microfibres and superabsorbent polymers, J. Intell. Mater. Syst. Struct. 25 (2014) 13–24.
[44] D. Snoeck, J. Dewanckele, V. Cnudde, N. De Belie, X-ray computed microtomography to study autogenous healing of cementitious materials promoted by superabsorbent polymers, Cem. Concr. Compos 65 (2016) 83–93, https://doi.org/10.1016/j.cemconcomp.2015.10.016.
[45] H.X.D. Lee, H.S. Wong, N.R. Buenfeld, Self-sealing of cracks in concrete using superabsorbent polymers, Cem. Concr. Res. 79 (2016) 194–208, https://doi.org/10.1016/j.cemconres.2015.09.008.
[46] J. Wang, J. Dewanckele, V. Cnudde, S. Van Vlierberghe, W. Verstraete, N. De Belie, X-ray computed tomography proof of bacterial-based self-healing in concrete, Cem. Concr. Compos 53 (2014) 289–304, https://doi.org/10.1016/j.cemconcomp.2014.07.014.
[47] E. Baffoe, A. Ghahremaninezhad, Effect of protein containing hydrogels on the self-healing of cementitious materials, J. Mater. Civ. Eng. 36 (2024), https://doi.org/10.1061/JMCEE7.MTENG-17025.
[48] H. Huang, G. Ye, D. Damidot, Effect of blast furnace slag on self-healing of microcracks in cementitious materials, Cem. Concr. Res. 60 (2014) 68–82, https://doi.org/10.1016/j.cemconres.2014.03.010.

[49] H. Huang, G. Ye, Self-healing of cracks in cement paste affected by additional Ca2 + ions in the healing agent, J. Intell. Mater. Syst. Struct. 26 (2015) 309–320, https://doi.org/10.1177/1045389×14525490.

[50] H. Huang, G. Ye, D. Damidot, Characterization and quantification of self-healing behaviors of microcracks due to further hydration in cement paste, Cem. Concr. Res. 52 (2013) 71–81, https://doi.org/10.1016/j.cemconres.2013.05.003.

[51] M.J. Krafcik, K.A. Erk, Characterization of superabsorbent poly (sodium-acrylate acrylamide) hydrogels and influence of chemical structure on internally cured mortar, Mater. Struct. 49 (2016) 4765–4778, https://doi.org/10.1617/s11527-016-0823-7.

[52] M.J. Krafcik, B. Bose, K.A. Erk, Synthesis and characterization of polymer-silica composite hydrogel particles and influence of hydrogel composition on cement paste microstructure, Adv. Civ. Eng. Mater. 7 (2018) 590–613, https://doi.org/10.1520/ACEM20170144.

[53] Q. Zhu, C.W. Barney, K.A. Erk, Effect of ionic crosslinking on the swelling and mechanical response of model superabsorbent polymer hydrogels for internally cured concrete, Mater. Struct. 48 (2015) 2261–2276, https://doi.org/10.1617/s11527-014-0308-5.

[54] M.J. Krafcik, N.D. Macke, K.A. Erk, Improved concrete materials with hydrogel-based internal curing agents, Gels 3 (2017) 46, https://doi.org/10.3390/gels3040046.

[55] Farzanian Khashayar, Ghahremaninezhad Ali, On the effect of chemical composition on the desorption of superabsorbent hydrogels in contact with a porous cementitious material, Gels 4 (2018) 70, https://doi.org/10.1617/s11527-017-1068-9.

[56] K. Farzanian, A. Ghahremaninezhad, Desorption of superabsorbent hydrogels with varied chemical compositions in cementitious materials, Mater. Struct. Mater. Et. Constr. 51 (2018), https://doi.org/10.1617/s11527-017-1128-1.

[57] K. Farzanian, A. Ghahremaninezhad, On the interaction between superabsorbent hydrogels and blended mixtures with supplementary cementitious materials, Adv. Civ. Eng. Mater. 7 (2018) 567–589.

[58] K. Farzanian, A. Ghahremaninezhad, On the effect of chemical composition on the desorption of superabsorbent hydrogels in contact with a porous cementitious material, Gels 4 (2018) 70, https://doi.org/10.1617/s11527-017-1068-9.

[59] K. Farzanian, A. Ghahremaninezhad, Desorption of superabsorbent hydrogels with varied chemical compositions in cementitious materials, Mater. Struct. (2017).

[60] D. Snoeck, Self-Healing and Microstructure of Cementitious Materials with Microfibres and Superabsorbent Polymers, 2016. ⟨http://studwww.ugent.be/~dsnoeck/PhD/PhDDidierSnoeck.pdf⟩.

[61] D. Snoeck, P. van den Heede, T. van Mullem, N. de Belie, Water penetration through cracks in self-healing cementitious materials with superabsorbent polymers studied by neutron radiography, Cem. Concr. Res. 113 (2018) 86–98, https://doi.org/10.1016/j.cemconres.2018.07.002.

[62] B. Vafaei, K. Farzanian, A. Ghahremaninezhad, The influence of superabsorbent polymer on the properties of alkali-activated slag pastes, Constr. Build. Mater. 236 (2020), https://doi.org/10.1016/j.conbuildmat.2019.117525.

[63] H. Huang, G. Ye, D. Damidot, Characterization and quantification of self-healing behaviors of microcracks due to further hydration in cement paste, Cem. Concr. Res. 52 (2013) 71–81, https://doi.org/10.1016/j.cemconres.2013.05.003.

[64] B. Lothenbach, G. Le Saout, M. Ben Haha, R. Figi, E. Wieland, Hydration of a low-alkali CEM III/B–SiO2 cement (LAC), Cem. Concr. Res. 42 (2012) 410–423.

[65] C. Hall, P. Barnes, A.D. Billimore, A.C. Jupe, X. Turrillas, Thermal decomposition of ettringite Ca 6 [Al (OH) 6] 2 (SO 4) 3· 26H 2 O, J. Chem. Soc. Faraday Trans. 92 (1996) 2125–2129.

[66] O. CHOwANIEC, Limestone addition in cement, EPFL (2012).

[67] O. CHOwANIEC, Limestone addition in cement, EPFL (2012).

[68] H. Huang, G. Ye, D. Damidot, Effect of blast furnace slag on self-healing of microcracks in cementitious materials, Cem. Concr. Res. 60 (2014) 68–82, https://doi.org/10.1016/j.cemconres.2014.03.010.

[69] M. Ben Haha, B. Lothenbach, G. Le Saout, F. Winnefeld, Influence of slag chemistry on the hydration of alkali-activated blast-furnace slag—Part II: effect of Al2O3, Cem. Concr. Res 42 (2012) 74–83.

[70] I. Halikia, L. Zoumpoulakis, E. Christodoulou, D. Prattis, Kinetic study of the thermal decomposition of calcium carbonate by isothermal methods of analysis, Eur. J. Miner. Process. Environ. Prot. 1 (2001) 89–102.

[71] E. Baffoe, A. Ghahremaninezhad, The effect of biomolecules on enzyme-induced calcium carbonate precipitation in cementitious materials, Constr. Build. Mater. 345 (2022) 128323, https://doi.org/10.1016/j.conbuildmat.2022.128323.

[72] M. Codina, C. Cau-dit-coumes, P. Le Bescop, J. Verdier, J.P. Ollivier, Design and characterization of low-heat and low-alkalinity cements, 38 (2008) 437–448. ⟨https://doi.org/10.1016/j.cemconres.2007.12.002⟩.

[73] V. Kocaba, Development and evaluation of methods to follow microstructural development of cementitious systems including slags, EPFL (2009).

[74] E. Schäfer, Einfluss der Reaktionen, verschiedener zementhauptbestandteile auf den alkalihaushalt der porenlösung des zementsteins, Verl. Bau und Tech. (2006).

[75] F. Glasser, M. Tyrer, K. Quillin, The chemistry of blended cements and backfills intended for use in radioactive waste disposal, Environ. Agency (1999).

[76] J.-I. Escalante-Garcia, J.H. Sharp, The chemical composition and microstructure of hydration products in blended cements, Cem. Concr. Compos 26 (2004) 967–976.

[77] K. Luke, E. Lachowski, Internal composition of 20-year-old fly ash and slag-blended ordinary Portland cement pastes, J. Am. Ceram. Soc. 91 (2008) 4084–4092.

[78] A.M. Harrisson, An examination of some pore and composite Portland cement pastes using scanning electron microscopy with X-ray analytical capability, Proc. 8th Int. Congr. Chem. Cem. 1986 (1986) 170–175.

[79] P. Chindasiriphan, H. Yokota, P. Pimpakan, Effect of fly ash and superabsorbent polymer on concrete self-healing ability, Constr. Build. Mater. 233 (2020) 116975, https://doi.org/10.1016/j.conbuildmat.2019.116975.

[80] M. Zhang, H. Zhang, D. Xu, L. Han, J. Zhang, L. Zhang, W. Wu, B. Tian, Removal of phosphate from aqueous solution using zeolite synthesized from fly ash by alkaline fusion followed by hydrothermal treatment, Sep Sci. Technol. 46 (2011) 2260–2274.

[81] S. Vichan, R. Rachan, S. Horpibulsuk, Strength and microstructure development in Bangkok clay stabilized with calcium carbide residue and biomass ash, Sci. 39 (2013) 186–193.

[82] S.W. Tang, X.H. Cai, Z. He, H.Y. Shao, Z.J. Li, E. Chen, Hydration process of fly ash blended cement pastes by impedance measurement, 113 (2016) 939–950. ⟨https://doi.org/10.1016/j.conbuildmat.2016.03.141⟩.

[83] K. Vance, G. Falzone, I. Pignatelli, M. Bauchy, M. Balonis, G. Sant, Direct Carbonation of Ca(OH)2 Using Liquid and Supercritical CO2: Implications for Carbon-Neutral Cementation, Ind. Eng. Chem. Res. 54 (2015) 8908–8918, https://doi.org/10.1021/acs.iecr.5b02356.

[84] P. Chindasiriphan, H. Yokota, P. Pimpakan, Effect of fly ash and superabsorbent polymer on concrete self-healing ability, Constr. Build. Mater. 233 (2020) 116975, https://doi.org/10.1016/j.conbuildmat.2019.116975.

[85] P. Yu, R.J. Kirkpatrick, B. Poe, P.F. McMillan, X. Cong, Structure of calcium silicate hydrate (C-S-H): near-, Mid-, and Far-infrared spectroscopy, J. Am. Ceram. Soc. 82 (1999) 742–748.

[86] S.C.B. Myneni, S.J. Traina, G.A. Waychunas, T.J. Logan, Vibrational spectroscopy of functional group chemistry and arsenate coordination in ettringite, Geochim Cosmochim. Acta 62 (1998) 3499–3514.

[87] S.J. Barnett, D.E. Macphee, E.E. Lachowski, N.J. Crammond, XRD, EDX and IR analysis of solid solutions between thaumasite and ettringite, Cem. Concr. Res. 32 (2002) 719–730.

[88] S.N. Ghosh, S.K. Handoo, Infrared and Raman spectral studies in cement and concrete, Cem. Concr. Res. 10 (1980) 771–782.

[89] S.C.B. Myneni, S.J. Traina, G.A. Waychunas, T.J. Logan, Vibrational spectroscopy of functional group chemistry and arsenate coordination in ettringite, Geochim Cosmochim. Acta 62 (1998) 3499–3514.

[90] S.J. Barnett, D.E. Macphee, E.E. Lachowski, N.J. Crammond, XRD, EDX and IR analysis of solid solutions between thaumasite and ettringite, Cem. Concr. Res. 32 (2002) 719–730.

[91] M. Xia, Z. Yao, L. Ge, T. Chen, H. Li, A potential bio-filler: the substitution effect of furfural modified clam shell for carbonate calcium in polypropylene, J. Compos Mater. 49 (2015) 807–816.

[92] K. Farzanian, B. Vafaei, A. Ghahremaninezhad, The behavior of superabsorbent polymers (SAPs) in cement mixtures with glass powders as supplementary cementitious materials, Materials 12 (2019), https://doi.org/10.3390/ma12213597.

[93] L. Fernández-Carrasco, D. Torrens-Martín, L.M. Morales, Sagrario Martínez-Ramírez, Infrared spectroscopy in the analysis of building and construction materials, Infrared Spectroscopy, Mater. Sci. Eng. 370 Technol. Technol. (2012) 369–382, https://doi.org/10.5772/36186.

[94] D.H. Chu, M. Vinoba, M. Bhagiyalakshmi, I.H. Baek, S.C. Nam, Y. Yoon, S.H. Kim, S.K. Jeong, CO2 mineralization into different polymorphs of CaCO3 using an aqueous-CO2 system, RSC Adv. 3 (2013) 21722–21729, https://doi.org/10.1039/C3RA44007A.

[95] M. Yousuf, A. Mollah, T.R. Hess, Y.-N. Tsai, D.L. Cocke, An FTIR and XPS investigations of the effects of carbonation on the solidification/stabilization of cement based systems-Portland type V with zinc, Cem. Concr. Res 23 (1993) 773–784.

[96] A.K. Parande, K. Stalin, R.K. Thangarajan, M.S. Karthikeyan, Utilization of Agroresidual Waste in Effective Blending in Portland Cement, 2011 (2011). ⟨https://doi.org/10.5402/2011/701862⟩.

[97] B. Yılmaz, A. Olgun, Studies on cement and mortar containing low-calcium fly ash, limestone, and dolomitic limestone, Cem. Concr. Compos 30 (2008) 194–201.

[98] C.M. Vladu, C. Hall, G.C. Maitland, Flow properties of freshly prepared ettringite suspensions in water at 25° C, J. Colloid Interface Sci. 294 (2006) 466–472.

[99] P. Mondal, S. Shah, L. Marks, Nanoscale characterization of cementitious materials, Acids Mater. J. 105 (2008) 174–179.

[100] H. Hoàng, J. Choi, K. Song, J. Song, J. Huh, B. Yeon, Self-healing properties of cement-based and alkali-activated slag-based fiber-reinforced composites 165 (2018) 801–811, https://doi.org/10.1016/j.conbuildmat.2018.01.023.

[101] S.-D. Wang, K.L. Scrivener, Hydration products of alkali activated slag cement, Cem. Concr. Res. 25 (1995) 561–571.

[102] C. Shi, R.L. Day, A calorimetric study of early hydration of alkali-slag cements, Cem. Concr. Res. 25 (1995) 1333–1346.

[103] J. Bijen, Benefits of slag and fly ash, Constr. Build. Mater. 10 (1996) 309–314, https://doi.org/10.1016/0950-0618(95)00014-3.

[104] K.V. Schuldyakov, L.Y. Kramar, B.Y. Trofimov, The properties of slag cement and its influence on the structure of the hardened cement paste, Procedia Eng. 150 (2016) 1433–1439.

[105] D. Homma, H. Mihashi, T. Nishiwaki, Self-healing capability of fibre reinforced cementitious composites, J. Adv. Concr. Technol. 7 (2009) 217–228.